Journal of *Marine Science and Engineering*

MDPI

Article

Integral Sliding Mode Output Feedback Control for Unmanned Marine Vehicles Using T–S Fuzzy Model with Unknown Premise Variables and Actuator Faults

Yang Wang [1], Xin Yang [1], Liying Hao [2,*], Tieshan Li [3,4] and C. L. (Philip) Chen [5]

1 College of Navigation, Dalian Maritime University, Dalian 116026, China; wangyang_youth@163.com (Y.W.)
2 Marine Electrical Engineering College, Dalian Maritime University, Dalian 116026, China
3 College of Automation Engineering, University of Electronic Science and Technology of China, Chengdu 611731, China; tieshanli@126.com
4 Yangtze Delta Region Institute, University of Electronic Science and Technology of China, Huzhou 313000, China
5 College of Computer Science and Engineering, South China University of Technology, Guangzhou 510006, China
* Correspondence: haoliying_0305@163.com

Abstract: This paper addresses integral sliding mode output feedback fault-tolerant control (FTC) of unmanned marine vessels (UMVs) with unknown premise variables and actuator faults. Due to the complexity of the marine environment, the presence of uncertainties in the yaw angle renders the premise variables in the Takagi–Sugeno (T–S) fuzzy model of UMVs unknown. Consequently, traditional integral sliding mode techniques become infeasible. To address this issue, a control strategy combining integral sliding mode based on output feedback with a compensator utilizing switching mechanisms is proposed. First, a radial basis function neural network is used to approximate the nonlinear terms in the UMV T–S fuzzy model. In addition, an integral sliding mode surface is constructed based on fault estimation information and membership function estimation. On this basis, an FTC scheme based on integral sliding mode output feedback is developed to ensure that the UMV system is asymptotically stable and satisfies the prescribed $\mathcal{H}_\infty$ performance index. Finally, simulation results are provided to demonstrate the effectiveness of the presented control strategy.

Keywords: unknown premise variables; integral sliding mode; output feedback control; Takagi–Sugeno (T–S) fuzzy models; unmanned marine vessels (UMVs)

Citation: Wang, Y.; Yang, X.; Hao, L.; Li, T.; Chen, C.L. Integral Sliding Mode Output Feedback Control for Unmanned Marine Vehicles Using T–S Fuzzy Model with Unknown Premise Variables and Actuator Faults. *J. Mar. Sci. Eng.* **2024**, *12*, 920. https://doi.org/10.3390/jmse12060920

Academic Editor: Mohamed Benbouzid

Received: 9 April 2024
Revised: 20 May 2024
Accepted: 21 May 2024
Published: 30 May 2024

1. Introduction

Unmanned marine vessels (UMVs) find wide applications across various domains, including tourism, fisheries, pollution cleanup, and more [1–7]. Compared with manned vessels, UMVs offer greater flexibility and adaptability. UMVs are influenced by disturbances in the maritime environment. These disturbances can cause vessels to deviate from their intended course or even lose stability. With increasing demands for precision and reliability in vessel motion, ensuring that vessels can perform various tasks stably and safely becomes crucial. In the literature, there are some excellent research results, including studies on sideslip angle control [8], trajectory tracking control [9], and heading control [10]. Additionally, dynamic positioning (DP) control is also a highly regarded research area, aiming to utilize thrust generated by its own propulsion system to counteract external disturbances and retain a specific orientation at a designated location on the sea surface, thereby fulfilling various operational functions [11–13]. DP systems can move freely in different marine environments and working conditions, without being restricted by anchor positions [14–19]. Alternatively, Takagi–Sugeno (T–S) fuzzy models boast robust approximation capabilities, enabling effective approximation of any smooth nonlinear function, making it an efficient method for nonlinear system modeling. Additionally, T–S

fuzzy models are subject to examination within the theoretical construct of fuzzy logic control, providing a flexible and effective tool for addressing control problems in complex systems. UMVs are typical complex nonlinear systems; the T–S fuzzy model stands out as an effective tool for designing controllers for such systems. Meanwhile, extensive research was conducted on the DP control problem based on the T–S fuzzy model [20–22]. Ref. [20] proposed a fuzzy controller design methodology to tackle the management of T–S fuzzy models dealing with multiplicative noise within nonlinear stochastic DP systems. In [21], a robust DP controller was developed utilizing T–S fuzzy models with H_∞ control techniques. In [22], a DP control scheme for UMVs was developed by using T–S fuzzy models. To tackle the trajectory tracking control issue of DP vessels amidst modeling uncertainties, environmental disturbances, and unpredictable velocities, ref. [23] combined performance control techniques with adaptive fuzzy backstepping control methods to design a novel adaptive fuzzy controller. In [24], a control strategy with high gain was given by combining the adaptive fuzzy method with the auxiliary dynamic system, considering the unknown parameters, unmeasured state, and saturated input of the ship dynamic model.

Despite that the aforementioned literature has yielded promising results, the controller may fail to operate effectively in the event of actuator faults. When UMVs operate in harsh marine environments, they are influenced by various uncertainties, including strong winds, large waves, marine pollution, and so on. These uncertainties exert additional pressure and loads on the actuators of vessels, making them more prone to failure. As noted in [25,26], occurrences of actuator faults can lead to significant performance degradation or mission cancellations. Fortunately, the fault-tolerant control (FTC) technology stands as an effective control methodology for addressing thruster failures. FTC denotes a system's capability to maintain its fundamental functions even if specific components fail. The premise of FTC lies in the system's redundancy, with the key being how to pre-design and utilize this redundancy effectively for fault tolerance. The approaches to achieve FTC mainly consist of two design methods: active FTC and passive FTC. The design principle of passive FTC aims to develop a fixed controller for anticipated faults, ensuring system stability and control performance while rendering the closed-loop system insensitive to faults. Due to the difficulty of implementing hardware redundancy in many practical control systems and its limited fault-tolerant capability, passive FTC methods may be challenging. Therefore, active FTC based on adaptive control methods is an effective approach. Its fundamental idea is to utilize adaptive mechanisms to estimate faults online, providing fault parameter information for controller design based on adaptive control methods [27–29]. Ref. [27] proposed an approach for fault-tolerant tracking control in T–S fuzzy model-based nonlinear systems, integrating integral sliding mode control (ISMC) with adaptive control techniques. In the work presented [28], a novel nonlinear robust FTC law is introduced for position tracking of a tilt tri-rotor unmanned aerial vehicle in the presence of unknown rear servo stuck faults, parametric uncertainties, and external disturbances. Ref. [29] introduced a novel approach for robust FTC of robot manipulators, employing an adaptive fuzzy ISMC and a disturbance observer. Ref. [30] focused on actuator fault mitigation, external disturbances, and actuator saturation in spacecraft. It proposed an FTC method based on adaptive integral sliding mode (ISM) to mitigate these issues. Ref. [31] investigated the issue of FTC for robots subjected to external disturbances, model uncertainties, and actuator faults. It suggested a control approach utilizing adaptive higher-order super-twisting control in conjunction with nonsingular terminal sliding mode. Ref. [32] addressed the DP control problem of unmanned ships with signal quantization. It designs an integral sliding mode FTC strategy [32–34]. We observe that the literature mentioned above suggests an integral sliding mode FTC scheme assuming the measurability of all system states. However, in reality, not all system states are entirely measurable. In such cases, designing an output feedback-based ISMC strategy is crucial for effectively controlling the system and achieving the desired performance. Ref. [33] suggested an FTC approach utilizing integral sliding mode output feedback for addressing ship propulsion failures and signal quantization concerns. An adaptive mechanism is employed to estimate fault information and upper

bounds of external disturbances online. Ref. [35] investigated ISM output feedback control methods, ensuring disturbance attenuation in linear systems. Addressing the issue of unknown state vectors, [33,36] designed ISMC with an output feedback component for UMVs. To mitigate the impact of actuator faults and failures on the system, ref. [34] proposed an observer-based fault estimation unit and designed an integral sliding mode output feedback FTC strategy. Unfortunately, when employing the T–S fuzzy model, the aforementioned results derived from the linear ship model become impractical. To the best of our knowledge, the utilization of an output ISMC framework in UMV T–S fuzzy systems has not been explored. Therefore, the main motivation of this study is to design the output ISMC law solely based on output measurements in the T–S fuzzy UMV model.

The T–S fuzzy model divides the input space into various fuzzy subspaces and constructs local linear models within each subspace to approximate nonlinear functions accurately. The ability to approximate complex nonlinear systems more effectively is facilitated by the property of piecewise linear approximation inherent in the T–S fuzzy modeling approach. In contrast with traditional methods, which linearize the model at a single operating point, the benefits of the T–S fuzzy model are apparent. Furthermore, extending linear system control methods to address the control problems of nonlinear systems based on T–S fuzzy modeling is another advantage. Leveraging these advantages, this paper applies the T–S fuzzy modeling approach to UMV models. The application of this method will provide more effective solutions for handling UMV DP systems in practical and complex marine environments. As far as we know, although there have been some excellent research results on the FTC of T–S fuzzy systems [14,22,37], ref. [37] suggested an FTC strategy that combines T–S fuzzy integral sliding mode adaptation with H_∞ performance, addressing the effects of thruster faults and marine disturbances on unmanned vessels. Ref. [38] proposed a fuzzy finite-time H_∞ mixed-trigger DP control strategy for UMV subjected to network attacks and ocean disturbances, utilizing a combination of fuzzy state observers and hybrid triggering techniques. To mitigate the effects of actuator faults and time-varying state delays on T–S fuzzy systems, a dynamic output feedback FTC strategy was formulated, incorporating fault estimation observers [39]. To address the simultaneous occurrence of sensor and actuator faults in nonlinear systems, ref. [40] proposed a T–S fuzzy FTC scheme based on proportional-integral observers, enabling the reconstruction of both sensor and actuator faults. Ref. [41] addressed the FTC problem of underwater vessels with actuator failures. Based on event-triggered techniques, it proposed a T–S fuzzy FTC method, aiming to ensure the efficient operation of underwater vessels while minimizing the waste of communication resources. It is noteworthy to mention that the aforementioned T–S fuzzy fault-tolerant controllers are all designed based on known premise variables. However, due to the complexity of the marine environment, there exists uncertainty in the yaw angle. In such scenarios, premise variables become challenging to measure, rendering traditional fuzzy controllers based on known premise variables ineffective. Fortunately, significant efforts have been made in addressing the problem of unknown premise variables in T–S fuzzy systems [42–44]. Refs. [42,43] addressed the challenges of fault detection and finite-frequency L_2–L_∞ filtering in T–S fuzzy systems with unknown membership functions, respectively. Ref. [44] investigated the decoupling of nonlinear dynamics to manage unmeasured states within the membership functions. Ref. [45] focused on addressing the fault detection issue of T–S fuzzy systems with partially unmeasurable premise variables and suggested a controller relying on observers. Ref. [46] introduced an output feedback fuzzy control approach grounded on observers for T–S fuzzy systems with partially unmeasurable premise variables. Ref. [47] presented a control methodology utilizing fuzzy observers, facilitating the regulation of nonlinear networked control systems amidst uncertain model parameters. To mitigate thruster failures and quantization effects in unmanned marine vessels modeled as T–S fuzzy systems with unmeasurable premise variables, ref. [48] devised a quantized sliding mode control strategy employing switching mechanisms. Although the FTC problem of the UMV considering unknown premise variables had been addressed [48], the inclusion of traditional sliding

mode control techniques based on state feedback in the literature fails to ensure robustness from the outset. Furthermore, the introduction of ISMC techniques, especially output ISMC techniques, presents new challenges for FTC of UMVs with unknown premise variables in T–S fuzzy systems. This increases control complexity, requiring the overcoming of challenges posed by unknown premise variables and the design of effective control methods suitable for the system. Therefore, another significant motivation for this research is to address the design of fault-tolerant controllers based on output ISM for T–S fuzzy UMVs in the presence of unknown premise variables.

Based on the foregoing analysis and discussion, this paper addresses the design of an FTC strategy based on ISM output feedback for a T–S fuzzy UMV model with unknown premise variables and actuator faults. A control strategy based on output feedback ISM with a compensator utilizing switching mechanisms is proposed, addressing the issue of unobservable premise variables. The RBFNN is utilized to estimate the nonlinear components within the T–S fuzzy model. Additionally, an adaptive mechanism is utilized to estimate fault information. Based on the estimated fault information and membership function estimation, an integral sliding mode surface is constructed. Expanding on this, a fault-tolerant control strategy is formulated using T–S fuzzy integral sliding mode output feedback to ensure the UMV system's asymptotic stability and fulfill the specified H_∞ performance criteria. The primary contributions are summarized as follows:

(1) This paper presents a novel approach by integrating an ISM output feedback technique into the design of a fault-tolerant controller for the T–S fuzzy UMV model, which enables the UMV T–S fuzzy system to achieve robustness against disturbances from the beginning only utilizing measurable output information.
(2) In contrast with the existing FTC approach applied to the T–S fuzzy UMV model [22,37], in response to the challenge posed by unknown premise variables in T–S fuzzy UMV models, this study devises compensators and fault-tolerant controllers based on a switching mechanism utilizing upper and lower bounds of membership functions, effectively reducing conservatism.
(3) Compared with the approaches for handling the nonlinear functions in the UMVs [48], this paper employs the radial basis function neural network (RBFNN) to approximate the nonlinear terms in the T–S fuzzy model of the UMV, which enhances the adaptability of the UMV system to complex marine environments, thereby improving its overall performance and robustness.

Then, the following structure of this manuscript is provided: In Section 2, we give the required definitions and existing results. Section 3 presents the FTC scheme based the output ISM method. In Section 4, the simulation results are provided. Section 5 presents the conclusions.

Notation: Let T^{-1}, T^T, and $T^\dagger$ denote the inverse, transpose , and pseudo-inverse of the matrix T, respectively. The notation diag $\{a_1, a_2, \ldots, a_n\}$ denotes a diagonal matrix containing the elements $a_1, a_2, \ldots, a_n$ along its main diagonal. The symbol "$*$" embedded within a matrix is employed to signify a term resulting from symmetry. $\mathcal{R}^n$ and $||z||$ represent Euclidean space with n-dimensions and the Euclidean norm of z, respectively.

2. Preliminaries

2.1. UMV System Model

The dynamic equation of the UMV with three degrees shown in [22] is as follows:

$$R\dot{v}(t) + Gv(t) + E\theta(t) = Nu^F(t) + d(t) \tag{1}$$

where for arbitrary Ξ, N [49] is defined as $N = \begin{bmatrix} 1 & 1 & 0 & 0 & 0 & \cos\Xi \\ 0 & 0 & 1 & 1 & 1 & \sin\Xi \\ k_1 & -k_2 & -k_3 & -k_4 & k_5 & k_6 \sin\Xi \end{bmatrix}$.
The meanings of other symbols in the equation are shown in Table 1. Correspondingly, the overall layout of the UMV is shown in Figure 1.

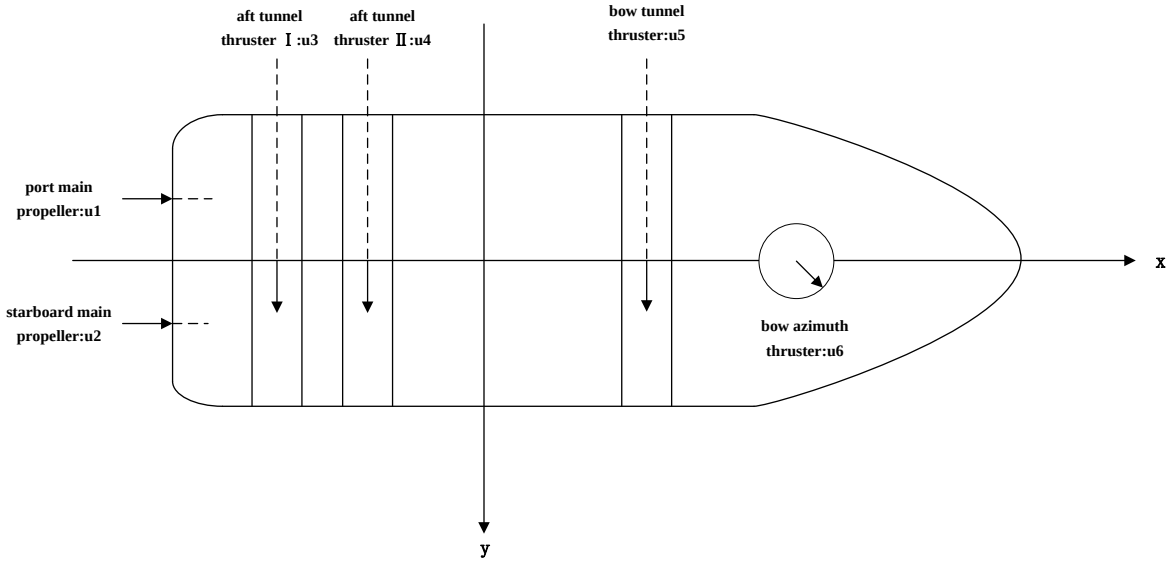

Figure 1. The overall layout of the UMV.

Table 1. Table of notations in the UMV model.

Symbols	Description
$v_1(t)$	surge velocity
$v_2(t)$	sway velocity
$v_3(t)$	yaw velocity
$\nu(t)$	$\nu(t) = \begin{bmatrix} v_1(t) & v_2(t) & v_3(t) \end{bmatrix}^T$
$(x_p(t), y_p(t))$	positions
$\phi(t)$	heading angle
$\theta(t)$	$\theta(t) = \begin{bmatrix} x_p(t) & y_p(t) & \phi(t) \end{bmatrix}^T$
R	inertia matrix
G	damping matrix
E	mooring forces matrix
N	thruster configuration matrix
$d(t)$	ocean disturbances, $\|d(t)\| \leqslant \bar{d}$
ϱ	unknown actuator effectiveness level matrix
$u_s(t)$	stuck fault with the property $\|u_s(t)\| \leqslant \bar{u}_s$
s	sth thruster, $s \in \{1, 2, \cdots, p\}$
t	tth malfunction mode, $t \in \{1, 2, \cdots, q\}$
$[\underline{\varrho}_s^t, \bar{\varrho}_s^t]$	$[\underline{\varrho}_s^t, \bar{\varrho}_s^t] \subseteq [0, 1]$
Δ_{ϱ^t}	$\{\varrho^t \mid \varrho^t = \text{diag}\{\varrho_1^t, \varrho_2^t, \ldots, \varrho_p^t\}, \varrho_s^t \in [\underline{\varrho}_s^t, \bar{\varrho}_s^t]\}$
Δ_{ς^t}	$\{\varsigma^t \mid \varsigma^t = \text{diag}\{\varsigma_1^t, \varsigma_2^t, \ldots, \varsigma_p^t\}, \varsigma_s^t = 0 \text{ or } 1\}$

The unified thruster fault model $u^F(t)$ is adopted as follows [25]:

$$u^F(t) = \varrho u(t) + \varsigma u_s(t) \tag{2}$$

with $\varrho \in \Delta_{\varrho^t}$, $\varsigma \in \Delta_{\varsigma^t}$.

The kinematic equation of the UMV is given as follows:

$$\dot{\theta}(t) = M(\phi(t))\nu(t), \tag{3}$$

with $M(\phi(t))$ being a rotation matrix defined in [22].

Let $\theta(t) = f(t, \nu)$ [14,25]. Then, from (1), we have the following:

$$\dot{\nu}(t) = \mathcal{A}\nu(t) + \mathcal{B}(\varrho u(t) + \varsigma u_s(t)) + \mathcal{D}d(t) + \mathcal{F}f(t, \nu) \tag{4}$$

where $\mathcal{A} = -R^{-1}G = \begin{bmatrix} a_{11} & a_{12} & a_{13} \\ a_{21} & a_{22} & a_{23} \\ a_{31} & a_{32} & a_{33} \end{bmatrix}$, $\mathcal{B} = -R^{-1}N = \begin{bmatrix} b_{11} & b_{12} & b_{13} & b_{14} & b_{15} & b_{16} \\ b_{21} & b_{22} & b_{23} & b_{24} & b_{25} & b_{26} \\ b_{31} & b_{32} & b_{33} & b_{34} & b_{35} & b_{36} \end{bmatrix}$, $\mathcal{D} = -R^{-1} = \begin{bmatrix} d_{11} & d_{12} & d_{13} \\ d_{21} & d_{22} & d_{23} \\ d_{31} & d_{32} & d_{33} \end{bmatrix}$, and $\mathcal{F} = -R^{-1}E = \begin{bmatrix} f_{11} & f_{12} & f_{13} \\ f_{21} & f_{22} & f_{23} \\ f_{31} & f_{32} & f_{33} \end{bmatrix}$.

2.2. T–S Fuzzy UMV Modeling

To streamline the presentation, we omit the independent variable t in the subsequent discussions.

Let $x = \begin{bmatrix} x_p & y_p & \phi & v_1 & v_2 & v_3 \end{bmatrix}^T$; we can obtain the following equation by combining (3) with (4):

$$\begin{aligned}
\dot{x}_p =& \cos(\phi)v_1 - \sin(\phi)v_2 \\
\dot{y}_p =& \sin(\phi)v_1 + \cos(\phi)v_2 \\
\dot{\phi} =& v_3 \\
\dot{v_1} =& a_{11}v_1 + a_{12}v_2 + a_{13}v_3 + b_{11}u_1^F + b_{12}u_2^F + b_{13}u_3^F + b_{14}u_4^F + b_{15}u_5^F + b_{16}u_6^F \\
&+ f_{11}f(t,v_1) + f_{12}f(t,v_2) + f_{13}f(t,v_3) + d_{11}d_1 + d_{12}d_2 + d_{13}d_3 \\
\dot{v_2} =& a_{21}v_1 + a_{22}v_2 + a_{23}v_3 + b_{21}u_1^F + b_{22}u_2^F + b_{23}u_3^F + b_{24}u_4^F + b_{25}u_5^F + b_{26}u_6^F \\
&+ f_{21}f(t,v_1) + f_{22}f(t,v_2) + f_{23}f(t,v_3) + d_{21}d_1 + d_{22}d_2 + d_{23}d_3 \\
\dot{v_3} =& a_{31}v_1 + a_{32}v_2 + a_{33}v_3 + b_{31}u_1^F + b_{32}u_2^F + b_{33}u_3^F + b_{34}u_4^F + b_{35}u_5^F + b_{36}u_6^F \\
&+ f_{31}f(t,v_1) + f_{32}f(t,v_2) + f_{33}f(t,v_3) + d_{31}d_1 + d_{32}d_2 + d_{33}d_3
\end{aligned} \tag{5}$$

In this study, the yaw angle $\phi(t)$ is considered as the premise variable, with its variation range supposed to be $-\frac{\pi}{6}$ to $\frac{\pi}{6}$ [22]. Denote $\sin(\phi), \cos(\phi)$ as ϖ_1, ϖ_2, respectively. Then, we can obtain the T–S fuzzy UMV model below.

Plant Rule i**:**

IF ϖ_1 is $\mathcal{M}_{i1}$ and ϖ_2 is $\mathcal{M}_{i2}$

THEN

$$\begin{cases} \dot{x} = A_i x + B(\varrho u + \varsigma u_s) + D_i d + F_i f(t,x) \\ y = C_i x \\ z = \overline{C}_i x \end{cases} \tag{6}$$

where $\mathcal{M}_{i1}$ and $\mathcal{M}_{i2}$ are fuzzy sets, $i = 1,2,3,4$; y, z are the measured output and the regulated output, respectively; $C_i, \overline{C}_i$ are known matrices, while $A_i = \begin{bmatrix} 0_{3\times3} & \mathscr{A}_i \\ 0_{3\times3} & \mathcal{A} \end{bmatrix}$, $B = \begin{bmatrix} 0_{3\times6} \\ \mathcal{B} \end{bmatrix}$, $D_i = \begin{bmatrix} 0_{3\times3} \\ \mathcal{D} \end{bmatrix}$, $F_i = \begin{bmatrix} 0_{3\times3} & 0_{3\times3} \\ 0_{3\times3} & \mathcal{F} \end{bmatrix}$, $\mathscr{A}_1 = \begin{bmatrix} 1 & -\frac{1}{2} & 0 \\ \frac{1}{2} & 1 & 0 \\ 0 & 0 & 1 \end{bmatrix}$, $\mathscr{A}_2 = \begin{bmatrix} \frac{\sqrt{3}}{2} & -\frac{1}{2} & 0 \\ \frac{1}{2} & \frac{\sqrt{3}}{2} & 0 \\ 0 & 0 & 1 \end{bmatrix}$, $\mathscr{A}_3 = \begin{bmatrix} 1 & \frac{1}{2} & 0 \\ -\frac{1}{2} & 1 & 0 \\ 0 & 0 & 1 \end{bmatrix}$, $\mathscr{A}_4 = \begin{bmatrix} \frac{\sqrt{3}}{2} & \frac{1}{2} & 0 \\ -\frac{1}{2} & \frac{\sqrt{3}}{2} & 0 \\ 0 & 0 & 1 \end{bmatrix}$. Define $y_d(t)$, which is a desired output; then the error is $\tilde{y} = y(t) - y_d(t)$. For convenience, let $y_d(t) = 0$, $\tilde{y} = y(t)$.

According to Formula (6), we have the following:

$$\begin{cases} \dot{x} = \sum_{i=1}^{4} h_i(\varpi)[A_i x + B(\varrho u + \varsigma u_s) + D_i d + F_i f(x)] \\ y = \sum_{i=1}^{4} h_i(\varpi) C_i x \\ z = \sum_{i=1}^{4} h_i(\varpi) \overline{C}_i x \end{cases} \tag{7}$$

where $\sum_{i=1}^{4} h_i(\varpi) = 1, h_i(\varpi) = \frac{\kappa_i(\varpi)}{\sum_{i=1}^{4} \kappa_i(\varpi)} \geqslant 0, \kappa_i(\varpi) = \mathcal{M}_{i1}(\varpi_1)\mathcal{M}_{i2}(\varpi_2)$.

2.3. RBFNN Approximation

To approximate the nonlinear term $f(x)$ over a compact set Ω in (7), the RBFNN [50] is introduced in this paper. Therefore, the following equation can be obtained:

$$f(x) = \omega^{*\mathrm{T}} \Xi(x) + \varphi \tag{8}$$

where

$$w^* = \arg\min_{\hat{w}} \left\{ \sup_{x \in \Omega} \left| f(x) - \hat{w}^T \Xi(x) \right| \right\} \in R^n$$

denotes the optimal weight vector, in which $\hat{w}$ represents the estimate of w^* and n means the number of the node; $\Xi(x) = [\xi_1(x), \xi_2(x), \cdots, \xi_n(x)]$ represents the radial basis function vector, the element $\xi_i(x)$ of which is usually chosen as the Gaussian function; and φ_0 is an unknown constant, which meets the following:

$$\| \varphi \| \leqslant \varphi_0 \tag{9}$$

Remark 1. *In contrast with [48], this paper employs adaptive RBFNN to approximate the nonlinearity $f(x)$ in (7). This approach simplifies the subsequent stability analysis by handling the nonlinear term more straightforwardly and enhances adaptability to unmodeled dynamics induced by complex and dynamic marine environments. It is worth mentioning that although we adopted the structure of the adaptive RBFNN mentioned above in this article, considering that the state in this article is not entirely obtainable, we used the estimated value of the state for the input information in the Gaussian basis function, which is to replace the original value with the estimated value for estimation; that is, we use $f(x) = \omega^{*\mathrm{T}} \Xi(\hat{x}) + \varphi$ to replace $f(x) = \omega^{*\mathrm{T}} \Xi(x) + \varphi$, where $\Xi(\hat{x}) = [\xi_1(\hat{x}), \xi_2(\hat{x}), \cdots, \xi_n(\hat{x})]$.*

2.4. Assumptions and Lemmas

Assumption 1. *In the event that partial or stuck faults occur in up to $p - i (i = 1, 2, \cdots, p-1)$, the remaining thrusters are capable of achieving the control target.*

Assumption 2. $\mathrm{Rank}(B\varrho) = \mathrm{Rank}(B) = l$ *for all* $\varrho \in \Delta_{\varrho^t}$.

Remark 2. *Assumption 1 above ensures that the feasible solution exists for the actuator failure accommodation problem of UMVs [25,48]. Assumption 2 ensures the presence of a feasible solution to the thruster fault accommodation issue [25,48].*

Lemma 1 ([25]). *For the full-rank decomposition in Equation (13), there exists $\mu > 0$ for $\forall \varrho \in \Delta_{\varrho^t}$, such that*

$$\bar{N} \varrho \bar{N}^{\mathrm{T}} \geq \mu \bar{N} \bar{N}^{\mathrm{T}}. \tag{10}$$

Lemma 2 ([51]). *For any $m \times n$ matrices C, D, and any scalars $\delta > 0$, $\lambda > 0$, the following inequalities are valid:*

$$C^T D + D^T C \leqslant \delta C^T C + \frac{1}{\delta} D^T D \tag{11}$$

$$\begin{bmatrix} 0 & C^T D \\ D^T C & 0 \end{bmatrix} \leqslant \begin{bmatrix} \lambda C^T C & 0 \\ 0 & \frac{1}{\lambda} D^T D \end{bmatrix} \tag{12}$$

3. Output Feedback-Based ISM FTC Strategy

In this section, an output feedback-based ISM surface and a switching-type fault-tolerant controller for the UMV will be provided. The proposed control scheme is given in Figure 2.

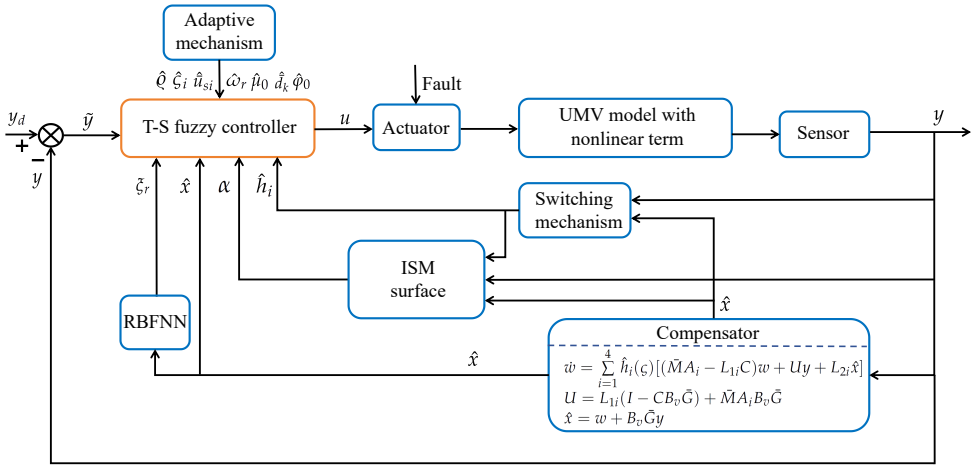

Figure 2. ISM output feedback-based FTC strategy for T–S UMV model.

3.1. Output ISM Surface Design

Suppose that matrix B can be decomposed into full-rank matrices in the following form [25]:

$$B = B_v \bar{N} \tag{13}$$

The ISM surface is provided as follows:

$$\alpha(y) = \bar{G}[y - y(t_0)] - \int_{t_0}^{t} \bar{N}\hat{\varrho}u_0(\tau)d\tau \tag{14}$$

where $\bar{G} = (CB_v)^{\dagger} - Y\left[I - (CB_v)(CB_v)^{\dagger}\right]$ is a freely designed matrix and $\hat{\varrho} = \text{diag}\{\hat{\varrho}_1, \hat{\varrho}_2, \ldots, \hat{\varrho}_p\}$ in (14) is the estimation of ϱ, which is updated by the following projection algorithms:

$$\dot{\hat{\varrho}}_i = \text{Proj}_{[\underline{\varrho}_i, \bar{\varrho}_i]}\{\beth\} = \begin{cases} 0, \text{ if } (\hat{\varrho}_i = \underline{\varrho}_i \text{ and } \beth \leqslant 0) \text{ or} (\hat{\varrho}_i = \bar{\varrho}_i \text{ and } \beth \geqslant 0) \\ \beth, \text{ otherwise} \end{cases} \tag{15}$$

where $\beth = \gamma_0 \alpha^{\mathrm{T}} \bar{N}^i \sum_{j=1}^{4} \hat{h}_j(\varpi) K_{ij} \hat{x}$, in which γ_0 is the adjusted parameter, $\bar{N}^i$ is the ith column of $\bar{N}$, and K_{ij} is the ith row of K in the jth fuzzy rule.

Remark 3. *In comparison with [48], this paper adopts output information instead of state information when designing the integral sliding surface, thereby reducing the reliance on unmeasurable state information. Additionally, the construction of the output integral sliding surface involves the unknown membership functions caused by unknown promise variables, undoubtedly posing greater challenges to the design of the integral sliding surface. To address this issue, compensators and controllers based on switching mechanisms will be elaborated in detail in the following text.*

The high gain compensator design is given as follows:

$$\begin{cases} \dot{w} = \sum_{i=1}^{4} \hat{h}_i(\varpi)[(\bar{M}A_i - L_{1i}C)w + Uy + L_{2i}\hat{x}] \\ U = L_{1i}(I - CB_v\bar{G}) + \bar{M}A_iB_v\bar{G} \\ \hat{x} = w + B_v\bar{G}y \end{cases}, \tag{16}$$

where $\bar{M} = I - B_v\bar{G}C$.

Theorem 1. *Consider the UMV (7) with satisfying Assumptions 1–2 and assume that the system is in the integral sliding surface (14). For given positive scalars $\gamma_d > 0, \beta_1 > 0$, if there exists $P_e = P_e^T > 0, P_x = P_x^T > 0, \bar{K}_i \in \mathcal{R}^{m\times n}$, that makes the following inequalities hold:*

$$\begin{bmatrix} \Pi_i & P_e\bar{M}D & \sum_{i=1}^{4}\left(h_i - \hat{h}_i\right)A_i^T\bar{M}^TP_e & T_2^TP_e \\ * & -\gamma_d^2 & 0 & 0 \\ * & * & -I & 0 \\ * & * & * & -\beta_1 \end{bmatrix} \leq 0 \tag{17}$$

where $\Pi_i = P_e\bar{M}A_i + A_i^T\bar{M}^TP_e - P_eA_iC^TC - \left(P_eA_iC^TC\right)^T$.

$$\begin{bmatrix} \Delta_i & P_x^{-1}\bar{C}^T & P_x^{-1}\sum_{i=1}^{4}\left(h_i - \hat{h}_i\right)A_i^T\bar{M}^T \\ * & -I & 0 \\ * & * & -\frac{1}{\beta_1} \end{bmatrix} \leq 0 \tag{18}$$

where $\Delta_i = \bar{M}A_iP_x^{-1} + P_x^{-1}A_i^T\bar{M}^T + P_e^{-1}\bar{C}^T\bar{C}A_i^T + \left(P_e^{-1}\bar{C}^T\bar{C}A_i^T\right)^T - B\hat{\varrho}\bar{K}_i - \left(B\hat{\varrho}\bar{K}_i\right)^T$, and the proposed dynamic compensator design (16) with the following:

$$\begin{aligned} K_i &= \bar{K}_iP_x \\ L_{1i} &= A_iC^T \\ L_{2i} &= P_e^{-1}C^TCA_i^TP_x \end{aligned}$$

can make the closed-loop system (26) and be asymptotically stable at the beginning and the $\mathcal{H}_\infty$ performance index is no more than γ_d.

Proof. The derivative of the ISM surface (14) is derived as follows:

$$\dot{\alpha}(y) = G\dot{y} - \bar{N}\hat{\varrho}u_0 \tag{19}$$

Substituting (7) into (19) results in the following:

$$\begin{aligned} \dot{\alpha}(y) = \sum_{i=1}^{4} h_i(\varpi)[&\bar{G}CA_ix + \bar{N}(\varrho - \hat{\varrho})u_0 + \bar{N}\varrho u_1 + \bar{N}\varsigma u_s \\ &+ \bar{G}CDd + \bar{N}E_0f(x)] \end{aligned} \tag{20}$$

Then we can obtain the following equivalent control: [52]

$$\begin{aligned} u_{1eq} = -\sum_{i=1}^{4} h_i(\varpi)(\bar{N}\varrho)^{\dagger}[&\bar{G}CA_ix + \bar{N}\varrho u_0 - \bar{N}\hat{\varrho}u_0 + \bar{N}\varsigma u_s \\ &+ \bar{G}CDd + \bar{N}E_0f(x)] \end{aligned} \tag{21}$$

Substituting (21) into (7) and using the property that $(N\varrho)(N\varrho)^{\dagger} = I_l$, then we can have the following equation:

$$\dot{x} = \sum_{i=1}^{4} h_i(\varpi)\{(I - B_v\bar{G}C)[A_i x + Dd] + B\hat{\varrho}u_0\} \tag{22}$$

Let $\bar{M} = I - B_v\bar{G}C, e = x - \hat{x}$; we have the following:

$$\dot{x} = \sum_{i=1}^{4} h_i(\varpi)\{\bar{M}A_i x + \bar{M}Dd + B\hat{\varrho}u_0\} \tag{23}$$

$$\begin{aligned} \dot{e} = &(\sum_{i=1}^{4} h_i\bar{M}A_i - \sum_{i=1}^{4}\hat{h}_i L_{1i}C)e + \sum_{i=1}^{4} h_i\bar{M}Dd \\ &+ (\sum_{i=1}^{4}\left(h_i - \hat{h}_i\right)\bar{M}A_i - \sum_{i=1}^{4}\hat{h}_i L_{2i})\hat{x}, \end{aligned} \tag{24}$$

$$\begin{aligned} \dot{\hat{x}} &= \sum_{i=1}^{4}\hat{h}_i[(\bar{M}A_i + L_{2i})\hat{x} + L_{1i}Ce] - B\hat{\varrho}\sum_{i=1}^{4}\hat{h}_i K_i\hat{x} \\ &= \sum_{i=1}^{4}\hat{h}_i[(\bar{M}A_i + L_{2i} - B\hat{\varrho}K_i)\hat{x} + L_{1i}Ce], \end{aligned} \tag{25}$$

where we defined that $x_e = \begin{bmatrix} \hat{x} \\ e \end{bmatrix}$, $A_{wi} = \begin{bmatrix} \bar{M}A_i + L_{2i} - B\hat{\varrho}K_i & L_{1i}C \\ \sum\limits_{i=1}^{4}\left(h_i - \hat{h}_i\right)\bar{M}A_i - L_{2i} & \sum\limits_{i=1}^{4} h_i\bar{M}A_i - L_{1i}C \end{bmatrix}$, $D_M = \begin{bmatrix} 0 \\ I \end{bmatrix}\bar{M}D = \begin{bmatrix} 0 \\ \bar{M}D \end{bmatrix}$, $C_{\hat{y}} = \begin{bmatrix} C & 0 \end{bmatrix}$, $C_{\hat{z}} = \begin{bmatrix} \bar{C} & 0 \end{bmatrix}$; then we have the following:

$$\begin{cases} \dot{x}_e = \sum\limits_{i=1}^{4}\hat{h}_i\{A_{wi}x_e + D_M d\} \\ \hat{y} = C_{\hat{y}}x_e \\ \hat{z} = C_{\hat{z}}x_e \end{cases} \tag{26}$$

Let $A_{1wi} = \begin{bmatrix} \bar{M}A_i + L_{2i} - B\hat{\varrho}K_i & L_{1i}C \\ -L_{2i} & \bar{M}A_i - L_{1i}C \end{bmatrix}$, $A_{2wi} = \sum\limits_{i=1}^{4}\left(h_i - \hat{h}_i\right)\begin{bmatrix} 0 & 0 \\ \bar{M}A_i & \bar{M}A_i \end{bmatrix}$; then the following equations can be derived:

$$\begin{cases} \dot{x}_e = \sum\limits_{i=1}^{4}\hat{h}_i\{(A_{1wi} + A_{2wi})x_e + D_M d\} \\ \hat{y} = C_{\hat{y}}x_e, \\ \hat{z} = C_{\hat{z}}x_e \end{cases} \tag{27}$$

Choosing the following Lyapunov function:

$$V_1 = x_e^T P x_e, \tag{28}$$

then we have the following:

$$\begin{aligned} \dot{V}_1 &= \dot{x}_e^T P x_e + x_e^T P\dot{x}_e \\ &= \sum_{i=1}^{4}\hat{h}_i\left\{x_e^T A_{wi}^T + d^T D_M^T\right\}Px_e + x_e^T P\sum_{i=1}^{4}\hat{h}_i\{A_{wi}x_e + D_M d\} \\ &= \sum_{i=1}^{4}\hat{h}_i\left\{x_e^T\left(A_{wi}^T P + PA_{wi}\right)x_e + d^T D_M^T P x_e + x_e^T P D_M d\right\} \end{aligned} \tag{29}$$

Due to the following:

$$d^T D_M^T P x_e + x_e^T P D_M d \le \gamma_d^{-2} x_e^T P D_M D_M^T P x_e + \gamma_d^2 d^T d, \tag{30}$$

Thus,

$$\begin{aligned} &\dot{V}_1 + \hat{z}^T \hat{z} - \gamma_d^2 d^T d \\ &\le \sum_{i=1}^{4} \hat{h}_i \left\{ x_e^T \left(A_{1wi}^T P + P A_{1wi} + \gamma_d^{-2} P D_M D_M^T P + C_{\hat{z}}^T C_{\hat{z}} \right) x_e + x_e^T \left(A_{2wi}^T P + P A_{2wi} \right) x_e \right\} \end{aligned} \tag{31}$$

Let $P = \begin{bmatrix} P_x & 0 \\ 0 & P_e \end{bmatrix}$; then we can get that $\gamma_d^{-2} P D_M D_M^T P = \begin{bmatrix} 0 & 0 \\ 0 & \gamma_d^{-2} P_e \bar{M} D D^T \bar{M}^T P_e \end{bmatrix}$, $C_{\hat{z}}^T C_{\hat{z}} = \begin{bmatrix} \bar{C}^T \bar{C} & 0 \\ 0 & 0 \end{bmatrix}$, so we can further get the following:

$$\begin{aligned} &x_e^T \left(A_{2wi}^T P + P A_{2wi} \right) x_e \\ &= \sum_{i=1}^{4} \left(h_i - \hat{h}_i \right) \left[\hat{x}^T A_i^T \bar{M}^T P_e e + e^T P_e \bar{M} A_i \hat{x} + e^T \left(A_i^T \bar{M}^T P_e + P_e \bar{M} A_i \right) e \right] \end{aligned} \tag{32}$$

$$\begin{aligned} e &= \begin{bmatrix} C \\ T_c \end{bmatrix}^{-1} \begin{bmatrix} C \\ T_c \end{bmatrix} e = \begin{bmatrix} C \\ T_c \end{bmatrix}^{-1} \begin{bmatrix} Ce \\ T_c e \end{bmatrix} = T_{cn} \begin{bmatrix} y - \hat{y} \\ T_c e \end{bmatrix} \\ &= T_1 y - T_1 \hat{y} + T_2 e \end{aligned} \tag{33}$$

where $T_1 = T_{cn} \begin{bmatrix} I \\ 0 \end{bmatrix}, T_2 = T_{cn} \begin{bmatrix} 0 \\ T_c \end{bmatrix}$.

Therefore,

$$e^T P_e \bar{M} A_i \hat{x} = y^T T_1^T P_e \bar{M} A_i \hat{x} - \hat{y}^T T_1^T P_e \bar{M} A_i \hat{x} + e^T T_2^T P_e \bar{M} A_i \hat{x} \tag{34}$$

$$\hat{x}^T A_i^T \bar{M}^T P_e e = \hat{x}^T A_i^T \bar{M}^T P_e T_1 y - \hat{x}^T A_i^T \bar{M}^T P_e T_1 \hat{y} + \hat{x}^T A_i^T \bar{M}^T P_e T_2 e \tag{35}$$

Let $\Lambda_i = y^T T_1^T P_e \bar{M} A_i \hat{x} - \hat{y}^T T_1^T P_e \bar{M} A_i \hat{x} + \hat{x}^T A_i^T \bar{M}^T P_e T_1 y - \hat{x}^T A_i^T \bar{M}^T P_e T_1 \hat{y}$,

$\bar{A}_{2wi} = \begin{bmatrix} 0 & \sum_{i=1}^{4} \left(h_i - \hat{h}_i \right) A_i^T \bar{M}^T P_e T_2 \\ \sum_{i=1}^{4} \left(h_i - \hat{h}_i \right) T_2^T P_e \bar{M} A_i & \sum_{i=1}^{4} \left(h_i - \hat{h}_i \right) \left(A_i^T \bar{M}^T P_e + P_e \bar{M} A_i \right) \end{bmatrix}$, $\begin{bmatrix} Q_{11} & Q_{12} \\ Q_{12}^T & Q_{22} \end{bmatrix} =$ $Q = A_{1wi}^T P + P A_{1wi} + \gamma_d^{-2} P D_M D_M^T P + C_{\hat{z}}^T C_{\hat{z}} + \bar{A}_{2wi}$, so we can get the following:

$$\dot{V}_1 + \hat{z}^T \hat{z} - \gamma_d^2 d^T d \le x_e^T \sum_{i=1}^{4} \hat{h}_i Q x_e + \sum_{i=1}^{4} \hat{h} \sum_{i=1}^{4} \left(h_i - \hat{h}_i \right) \Lambda_i \tag{36}$$

Thus, to make $\dot{V}_1 + \hat{z}^T \hat{z} - \gamma_d^2 d^T d \le 0$ hold, simply prove the following:

$$\begin{cases} \sum_{i=1}^{4} \hat{h}_i \begin{bmatrix} Q_{11} & Q_{12} \\ Q_{21} & Q_{22} \end{bmatrix} \le 0 \\ \hat{h}_i = \begin{cases} \bar{h}_i, \Lambda_i > 0 \\ \underline{h}_i, \Lambda_i \le 0 \end{cases} \end{cases}, \tag{37}$$

where

$$\begin{aligned}
Q_{11} &= P_x\bar{M}A_i + A_i^T\bar{M}^TP_x + P_xL_{2i} + L_{2i}^TP_x - P_xB\hat{\varrho}K_i - (P_xB\hat{\varrho}K_i)^T + \bar{C}^T\bar{C} \\
Q_{12} &= P_xL_{1i}C - L_{2i}^TP_e + \sum_{i=1}^{4}\left(h_i - \hat{h}_i\right)A_i^T\bar{M}^TP_eT_2 \\
Q_{22} &= P_e(\bar{M}A_i - L_{1i}C) + (\bar{M}A_i - L_{1i}C)^TP_e + \gamma_d^{-2}P_e\bar{M}DD^T\bar{M}^TP_e \\
&\quad + \sum_{i=1}^{4}\left(h_i - \hat{h}_i\right)\left(A_i^T\bar{M}^TP_e + P_e\bar{M}A_i\right).
\end{aligned}$$

Remark 4. *Formula (37) provides a switching function to provide estimation information for the membership function. Compared with the switching mechanism in reference [48], the switching function provided in this paper can effectively utilize the upper and lower bounds of the membership function, reducing conservatism.*

According to $L_{1i} = A_iC^T$, $L_{2i} = P_e^{-1}C^TCA_i^TP_x$; then $Q_{12} = \sum_{i=1}^{4}\left(h_i - \hat{h}_i\right)A_i^T\bar{M}^TP_eT_2$.

It follows from Lemma 2 that

$$\begin{aligned}
\begin{bmatrix} Q_{11} & Q_{12} \\ Q_{12}^T & Q_{22} \end{bmatrix} &= \begin{bmatrix} Q_{11} & \sum_{i=1}^{4}\left(h_i - \hat{h}_i\right)A_i^T\bar{M}^TP_eT_2 \\ \sum_{i=1}^{4}\left(h_i - \hat{h}_i\right)T_2^TP_e\bar{M}A_i & Q_{22} \end{bmatrix} \\
&\leq \begin{bmatrix} Q_{11} + \beta_1\sum_{i=1}^{4}\left(h_i - \hat{h}_i\right)A_i^T\bar{M}^T\bar{M}A_i & 0 \\ 0 & Q_{22} + \frac{1}{\beta_1}T_2^TP_eP_eT_2 \end{bmatrix}, \\
&= \tilde{Q} = \begin{bmatrix} \tilde{Q}_{11} & \tilde{Q}_{12} \\ \tilde{Q}_{12}^T & \tilde{Q}_{22} \end{bmatrix}
\end{aligned} \tag{38}$$

namely,

$$\begin{aligned}
\tilde{Q}_{11} =& P_x\bar{M}A_i + A_i^T\bar{M}^TP_x + P_xL_{2i} + L_{2i}^TP_x - P_xB\hat{\varrho}K_i - (P_xB\hat{\varrho}K_i)^T + \bar{C}^T\bar{C} \\
&+ \beta_1\sum_{i=1}^{4}\left(h_i - \hat{h}_i\right)A_i^T\bar{M}^T\bar{M}A_i \\
\tilde{Q}_{22} =& P_e\bar{M}A_i - P_eA_iC^TC + \left(P_e\bar{M}A_i - P_eA_iC^TC\right)^T + \gamma_d^{-2}P_e\bar{M}DD^T\bar{M}^TP_e \\
&+ \sum_{i=1}^{4}\left(h_i - \hat{h}_i\right)\left(A_i^T\bar{M}^TP_e + P_e\bar{M}A_i\right) + \frac{1}{\beta_1}T_2^TP_eP_eT_2
\end{aligned} \tag{39}$$

To prove $Q \leq 0$, as long as $\tilde{Q}_{11} \leq 0$ and $\tilde{Q}_{22} \leq 0$, it can be inferred through contract transformation and Schur's complement lemma that $\tilde{Q}_{11} \leq 0$ and $\tilde{Q}_{22} \leq 0$ are equivalent to the following two linear matrix inequalities in Theorem 1.

The proof of Theorem 1 is complete. □

3.2. ISM Output Feedback Controller Design

The ISM controller is designed as follows:

$$u = u_0 + u_1 \tag{40}$$

where

$$\begin{aligned} u_0 &= \sum_{i=1}^{4} \hat{h}_i(\varpi) K_i \hat{x} \\ u_1 &= -\zeta \hat{\mu}_0 \bar{N}^{\mathrm{T}} \frac{\alpha(y)}{\|\alpha(y)\|} \end{aligned} \tag{41}$$

where $K_i = \bar{K}_i P_x, \bar{K}_i \in \mathcal{R}^{m\times n}$ $(i = 1,2,3,4)$, and $P_x \in \mathcal{R}^{n\times n}$; $\hat{\mu}_0$ is an approximation of μ_0 with the relation that $\mu_0 = \frac{1}{\mu}$, in which the parameter μ is introduced from Lemma 1, while

$$\begin{aligned} \zeta =& \frac{1}{\lambda_{\bar{N}}} \Bigg(\|\bar{N}\| \|E_0\| \hat{\varphi}_0 + \|\bar{N}\| \|E_0\| \sum_{r=1}^{M} \hat{\omega}_r \xi_r(\hat{x}) \\ &+ \sum_{i=1}^{m} \|\bar{N}_i\| \hat{\varsigma}_i \hat{\bar{u}}_{si} + \sum_{k=1}^{q} \left\|\bar{G} C D_k\right\| \hat{\bar{d}}_k + \epsilon \Bigg) \end{aligned} \tag{42}$$

where $\lambda_{\bar{N}}$ is the smallest eigenvalue of $\bar{N}\bar{N}^T$, $\epsilon > 0$, while $\hat{\varphi}_0, \hat{\omega}, \hat{\varsigma}, \hat{\bar{u}}_s$, and $\hat{\bar{d}}$ represent the estimations of φ_0, ω, ς, $\bar{u}_s$, and $\bar{d}$, respectively.

For further analysis, the matrix decomposed forms are given as [37].

In addition, the adaptive laws are shown as follows:

$$\begin{aligned} &\dot{\hat{\mu}}_0 = \gamma \zeta \lambda_N \|\alpha(y)\|, \dot{\hat{\bar{d}}}_k = \gamma_{3k} \|\alpha(y)\| \left\|\bar{G} C D_k\right\|, \\ &\dot{\hat{\bar{u}}}_{si} = \gamma_{1i} \|\alpha(y)\| \|\bar{N}_i\|, \dot{\hat{\omega}}_r = \gamma_{4r} \|\alpha(y)\| \|\bar{N}\| \|E_0\| \xi_r(\hat{x}), \\ &\dot{\hat{\varsigma}}_i = \gamma_{2i} \|\alpha(y)\| \|\bar{N}_i\| \hat{\bar{u}}_{si}, \dot{\hat{\varphi}}_0 = \gamma_5 \|\alpha(y)\| \|\bar{N}\| \|E_0\|, \\ &\hat{\mu}_0(0) = \mu_{00}, \quad \hat{\bar{u}}_{si}(0) = \bar{u}_{si0}, \quad \hat{\varsigma}_i(0) = \varsigma_{i0}, \\ &\hat{\bar{d}}_k(0) = \bar{d}_{k0}, \quad \hat{\omega}_r(0) = \omega_{r0}, \quad \hat{\varphi}_0(0) = \varphi_{00}. \end{aligned} \tag{43}$$

where ζ is as shown in (42); $\mu_{00}, \bar{u}_{si0}, \varsigma_{i0}, \hat{\bar{d}}_{k0}, \omega_{r0}$, and φ_{00} are bounded initial values of $\hat{\mu}_0, \hat{\bar{u}}_{si}, \hat{\varsigma}_i, \hat{\bar{d}}_k, \hat{\omega}_r$, and $\hat{\varphi}_0$, respectively. The design parameters $\gamma, \gamma_{1i}, \gamma_{2i}, \gamma_{3k}, \gamma_{4r}$, and γ_5 are positive.

We define the following:

$$\begin{aligned} &\tilde{\mu}_0 = \hat{\mu}_0 - \mu_0, \tilde{\varrho} = \hat{\varrho} - \varrho, \tilde{\omega} = \hat{\omega} - \omega, \\ &\tilde{\bar{u}}_s = \hat{\bar{u}}_s - \bar{u}_s, \tilde{\bar{d}} = \hat{\bar{d}} - \bar{d}, \\ &\tilde{\varphi}_0 = \hat{\varphi}_0 - \varphi_0, \tilde{\varsigma} = \hat{\varsigma} - \varsigma. \end{aligned} \tag{44}$$

Obviously, we can further derive the following:

$$\begin{aligned} &\dot{\tilde{\mu}}_0 = \dot{\hat{\mu}}_0, \dot{\tilde{\varrho}} = \dot{\hat{\varrho}}, \dot{\tilde{\omega}} = \dot{\hat{\omega}}, \dot{\tilde{\bar{u}}}_s = \dot{\hat{\bar{u}}}_s, \\ &\dot{\tilde{\bar{d}}} = \dot{\hat{\bar{d}}}, \dot{\tilde{\varphi}}_0 = \dot{\hat{\varphi}}_0, \dot{\tilde{\varsigma}} = \dot{\hat{\varsigma}}. \end{aligned} \tag{45}$$

Now, the following theorem is given to analyze the reachability of the output ISM.

Theorem 2. *Suppose that the linear matrix inequalities (17) and (18) in Theorem 1 have feasible solutions. Then, the state of the system (7) onto the ISM surface* $\Omega \triangleq \{y \in \mathcal{R}^m : \alpha(y) = 0\}$ *can be driven by the ISMC law (41) and the adaptive laws (43).*

Proof. Let $\tilde{\alpha} = \left[\alpha^{\mathrm{T}}, \tilde{\varrho}^{\mathrm{T}}, \tilde{\mu}_0^{\mathrm{T}}, \tilde{u}_s^{\mathrm{T}}, \tilde{\zeta}^{\mathrm{T}}, \tilde{\tilde{d}}_k^{\mathrm{T}}, \tilde{\omega}^{\mathrm{T}}, \tilde{\varphi}_0^{\mathrm{T}}\right]^{\mathrm{T}}$; then we have the candidate Lyapunov function below:

$$\begin{aligned} V(\tilde{\alpha}) =& V_0 + \frac{1}{2}\gamma^{-1}\mu\tilde{\mu}_0^2 + \sum_{i\in\bar{M}}\frac{\tilde{\varrho}_i^2}{2\gamma_{0i}} + \sum_{i\in\bar{M}}\frac{\varsigma_i\tilde{u}_{si}^2}{2\gamma_{1i}} \\ &+ \sum_{i\in\bar{M}}\frac{\tilde{\zeta}_i^2}{2\gamma_{2i}} + \sum_{k\in\bar{Q}}\frac{\tilde{\tilde{d}}_k^2}{2\gamma_{3k}} + \sum_{r\in\bar{P}}\frac{\tilde{\omega}_r^2}{2\gamma_{4r}} + \frac{\tilde{\varphi}_0^2}{2\gamma_5} \end{aligned} \tag{46}$$

where $V_0 = (1/2)\alpha^{\mathrm{T}}(y)\alpha(y)$.

Deriving the following derivative of V_0 by substituting the system (7):

$$\begin{aligned} \dot{V}_0 = \alpha^{\mathrm{T}}(y)\dot{\alpha}(y) =& \alpha^T(y)[\bar{G}C\sum_{i=1}^{4}h_i(\omega)A_ix + \bar{N}(\varrho-\hat{\varrho})u_0 + \bar{N}\varrho u_1 \\ &+ \bar{N}\varsigma u_s + \bar{G}CDd + \bar{G}CFf(x)] \end{aligned} \tag{47}$$

The following text will abbreviate $\alpha(y)$ as α. According to Assumption 1, it is not difficult to obtain the following inequalities:

$$\begin{aligned} \alpha^{\mathrm{T}}\bar{G}CDd &= \sum_{k\in\bar{Q}}\alpha^{\mathrm{T}}\bar{G}CD_kd_k \le \sum_{k\in\bar{Q}}\|\alpha\|\left\|\bar{G}CD_k\right\|\bar{d}_k \\ \alpha^{\mathrm{T}}\bar{N}\varsigma u_s &= \sum_{i\in\bar{M}}\alpha^{\mathrm{T}}\bar{N}_i\varsigma_iu_{si} \le \sum_{i\in\bar{M}}\|\alpha\|\|\bar{N}_i\|\varsigma_i\|u_{si}\| \le \sum_{i\in\bar{M}}\|\alpha\|\|\bar{N}_i\|\varsigma_i\bar{u}_{si} \end{aligned} \tag{48}$$

Based on (47) and (48), we can show the following:

$$\dot{V}_0 \le \alpha^{\mathrm{T}}\bar{N}\varrho u_1 + \alpha^{\mathrm{T}}\bar{N}E_0f(x) - \alpha^{\mathrm{T}}\bar{N}\tilde{\varrho}u_0 + \sum_{i\in\bar{M}}\|\alpha\|\|\bar{N}_i\|\varsigma_i\bar{u}_{si} + \sum_{k\in\bar{Q}}\|\alpha\|\left\|\bar{G}CD_k\right\|\bar{d}_k$$

From (41), we can further get the following:

$$\begin{aligned} \dot{V}_0 \le& -\alpha^{\mathrm{T}}\bar{N}\varrho\zeta\hat{\mu}_0\bar{N}^{\mathrm{T}}\frac{\alpha}{\|\alpha\|} + \sum_{i\in\bar{M}}\|\alpha\|\|\bar{N}_i\|\varsigma_i\bar{u}_{si} + \alpha^{\mathrm{T}}\bar{N}E_0f(x) \\ &+ \sum_{k\in\bar{Q}}\|\alpha\|\left\|\bar{G}CD_k\right\|\bar{d}_k - \alpha^{\mathrm{T}}\bar{N}\tilde{\varrho}\sum_{i=1}^{4}\hat{h}_i(\varpi)K_i\hat{x} \end{aligned} \tag{49}$$

We have the following inequality by substituting (44) into (49) according to [50] the following:

$$\begin{aligned} \dot{V}_0 \le& -\alpha^{\mathrm{T}}\bar{N}\varrho\zeta\hat{\mu}_0\bar{N}^{\mathrm{T}}\frac{\alpha}{\|\alpha\|} + \sum_{i\in\bar{M}}\|\alpha\|\|\bar{N}_i\|\hat{\varsigma}_i\hat{\bar{u}}_{si} - \sum_{i\in\bar{M}}\|\alpha\|\|\bar{N}_i\|\tilde{\varsigma}_i\hat{\bar{u}}_{si} \\ &- \sum_{i\in\bar{M}}\|\alpha\|\|\bar{N}_i\|\varsigma_i\tilde{\bar{u}}_{si} + \sum_{k\in\bar{Q}}\|\alpha\|\left\|\bar{G}CD_k\right\|\hat{\tilde{d}}_k - \sum_{k\in\bar{Q}}\|\alpha\|\left\|\bar{G}CD_k\right\|\tilde{\tilde{d}}_k \\ &- \alpha^{\mathrm{T}}\bar{N}\tilde{\varrho}\sum_{i=1}^{4}\hat{h}_i(\varpi)K_i\hat{x} + \alpha^{\mathrm{T}}\bar{N}E_0\left(\omega^{\mathrm{T}}\xi(x) + \varphi(x)\right) \end{aligned} \tag{50}$$

Obviously,

$$\begin{aligned} \alpha^{\mathrm{T}}\bar{N}E_0\left(\omega^{\mathrm{T}}\xi(x) + \varphi(x)\right) &\le \|\alpha\|\|\bar{N}\|\|E_0\|\left(\omega^{\mathrm{T}}\xi(x) + \|\varphi(x)\|\right) \\ &\le \|\alpha\|\|\bar{N}\|\|E_0\|\left(\sum_{r=1}^{\bar{P}}\omega_r\xi_r(x) + \varphi_0\right) \end{aligned} \tag{51}$$

We can achieve the following inequality by combining (50) with (51):

$$\begin{aligned}\dot{V}_0 \leq & -\alpha^{\mathrm{T}}\bar{N}\varrho\zeta\hat{\mu}_0\bar{N}^{\mathrm{T}}\frac{\alpha}{\|\alpha\|}+\sum_{i\in\bar{M}}\|\alpha\|\|\bar{N}_i\|\hat{\varsigma}_i\hat{u}_{si}-\sum_{i\in\bar{M}}\|\alpha\|\|\bar{N}_i\|\tilde{\varsigma}_i\hat{u}_{si}\\ & -\sum_{i\in\bar{M}}\|\alpha\|\|\bar{N}_i\|\varsigma_i\tilde{u}_{si}+\sum_{k\in\bar{Q}}\|\alpha\|\left\|\bar{G}CD_k\right\|\hat{\bar{d}}_k-\sum_{k\in\bar{Q}}\|\alpha\|\left\|\bar{G}CD_k\right\|\tilde{\bar{d}}_k\\ & -\sum_{j=1}^{4}\hat{h}_j(\varpi)\sum_{i\in\bar{M}}\alpha^{\mathrm{T}}\bar{N}^i\tilde{\varrho}_iK_{ij}\hat{x}+\|\alpha\|\|\bar{N}\|\|E_0\|\left(\sum_{r\in\bar{P}}\omega_r\xi_r(x)+\varphi_0\right)\end{aligned} \tag{52}$$

From (44) and (52), we can get the following:

$$\begin{aligned}\dot{V}_0 \leq & -\alpha^{\mathrm{T}}\bar{N}\varrho\zeta\hat{\mu}_0\bar{N}^{\mathrm{T}}\frac{\alpha}{\|\alpha\|}+\sum_{i\in\bar{M}}\|\alpha\|\|\bar{N}_i\|\hat{\varsigma}_i\hat{u}_{si}-\sum_{i\in\bar{M}}\|\alpha\|\|\bar{N}_i\|\tilde{\varsigma}_i\hat{u}_{si}\\ & -\sum_{i\in\bar{M}}\|\alpha\|\|\bar{N}_i\|\varsigma_i\tilde{u}_{si}+\sum_{k\in\bar{Q}}\|\alpha\|\left\|\bar{G}CD_k\right\|\hat{\bar{d}}_k-\sum_{j=1}^{4}\hat{h}_j(\varpi)\sum_{i\in\bar{M}}\alpha^{\mathrm{T}}\bar{N}^i\tilde{\varrho}_iK_{ij}\hat{x}\\ & +\|\alpha\|\|\bar{N}\|\|E_0\|\left(\sum_{r\in\bar{P}}\hat{\omega}_r\xi_r(x)-\tilde{\omega}^{\mathrm{T}}\xi(x)+\hat{\varphi}_0-\tilde{\varphi}_0\right)-\sum_{k\in\bar{Q}}\|\alpha\|\left\|\bar{G}CD_k\right\|\tilde{\bar{d}}_k\end{aligned} \tag{53}$$

Obviously, $\hat{\mu}_0(t) > 0$. The following inequality can be derived from Lemma 1:

$$-\zeta\hat{\mu}_0\alpha^{\mathrm{T}}N\varrho N^{\mathrm{T}}\frac{\alpha}{\|\alpha\|}\leq-\zeta\hat{\mu}_0\mu\lambda_N\|\alpha\|$$

Now, it is easy to get from (53) the following:

$$\begin{aligned}\dot{V}_0 \leq & -\zeta(\hat{\mu}_0+\tilde{\mu}_0)\mu\lambda_N\|\alpha\|+\sum_{i\in\bar{M}}\|\alpha\|\|\bar{N}_i\|\hat{\varsigma}_i\hat{u}_{si}-\sum_{i\in\bar{M}}\|\alpha\|\|\bar{N}_i\|\tilde{\varsigma}_i\hat{u}_{si}\\ & -\sum_{i\in\bar{M}}\|\alpha\|\|\bar{N}_i\|\varsigma_i\tilde{u}_{si}+\sum_{k\in\bar{Q}}\|\alpha\|\left\|\bar{G}CD_k\right\|\hat{\bar{d}}_k-\sum_{k\in\bar{Q}}\|\alpha\|\left\|\bar{G}CD_k\right\|\tilde{\bar{d}}_k\\ & +\|\alpha\|\|\bar{N}\|\|E_0\|\left(\sum_{r\in\bar{P}}\hat{\omega}_r\xi_r(x)-\tilde{\omega}^{\mathrm{T}}\xi(x)+\hat{\varphi}_0-\tilde{\varphi}_0\right)\\ & -\sum_{j=1}^{4}\hat{h}_j(\varpi)\sum_{i\in\bar{M}}\alpha^{\mathrm{T}}\bar{N}^i\tilde{\varrho}_iK_{ij}\hat{x}\end{aligned} \tag{54}$$

Substituting (42) into (54), we get the following:

$$\begin{aligned}\dot{V}_0 \leq & -\epsilon\|\alpha\|-\zeta\tilde{\mu}_0\mu\lambda_N\|\alpha\|-\sum_{k\in\bar{Q}}\|\alpha\|\left\|\bar{G}CD_k\right\|\tilde{\bar{d}}_k-\|\alpha\|\|\bar{N}\|\|E_0\|\sum_{r\in\bar{P}}\tilde{\omega}_r\xi_r(x)\\ & -\|\alpha\|\|\bar{N}\|\|E_0\|\tilde{\varphi}_0-\sum_{i\in\bar{M}}\|\alpha\|\|\bar{N}_i\|\tilde{\varsigma}_i\hat{u}_{si}-\sum_{i\in\bar{M}}\|\alpha\|\|\bar{N}_i\|\varsigma_i\tilde{u}_{si}\\ & -\sum_{j=1}^{4}\hat{h}_j(\varpi)\sum_{i\in\bar{M}}\alpha^{\mathrm{T}}\bar{N}^i\tilde{\varrho}_iK_{ij}\hat{x}\end{aligned}$$

Considering the adaptive laws (43) and (45), we have the following derivative of (46):

$$\begin{aligned}\dot{V}(\tilde{\alpha}) = & \dot{V}_0+\sum_{i\in\bar{M}}\frac{\tilde{\varrho}_i\dot{\tilde{\varrho}}_i}{\gamma_{0i}}+\gamma^{-1}\mu\tilde{\mu}_0\dot{\tilde{\mu}}_0+\sum_{i\in\bar{M}}\frac{\varsigma_i\tilde{\bar{u}}_{si}\dot{\tilde{\bar{u}}}_{si}}{\gamma_{1i}}+\\ & \sum_{i\in\bar{M}}\frac{\tilde{\varsigma}_i\dot{\tilde{\varsigma}}_i}{\gamma_{2i}}+\sum_{k\in\bar{Q}}\frac{\tilde{\bar{d}}_k\dot{\tilde{\bar{d}}}_k}{\gamma_{3k}}+\sum_{r\in\bar{P}}\frac{\tilde{\omega}_r\dot{\tilde{\omega}}_r}{\gamma_{4r}}+\frac{\tilde{\varphi}_0\dot{\tilde{\varphi}}_0}{\gamma_5}\end{aligned} \tag{55}$$

From (43), we have $-\zeta\mu\lambda_N\tilde{\mu}_0\|\beta\| + \gamma^{-1}\mu\tilde{\mu}_0\dot{\tilde{\mu}}_0 = 0$. Thus, from (55), we can get $\dot{V}(\tilde{\alpha}) \leq -\epsilon\|\alpha\| \leq 0$. Further, $V(\tilde{\alpha}) \leq V(\tilde{\alpha}(0)) \triangleq V_0$ is valid. Then, we can obtain the following inequality by simultaneously integrating both the left and right sides of (55):

$$V - V(0) \leq -\int_0^t \epsilon\|\alpha\|\mathrm{d}t \tag{56}$$

From the inequality above, it is obvious that $\int_0^\infty \epsilon\|\alpha\|dt \leq V_0 - V_\infty < \infty$ is valid, that is, $\alpha \in \mathcal{L}_2 \bigcap \mathcal{L}_\infty$. Hence, utilizing Barbalat's lemma ensures that the system trajectories are confined to the ISM surface. □

4. Simulation Result

In this section, the results are shown to demonstrate the effectiveness of the proposed control strategy for UMVs. The parameter matrices R, G, E, N of the UMV model are obtained from [21,22]. The simulated propulsion layout reference is Figure 1.

From [22], we have the following: $\begin{cases} d_1 = 0.27\mathbb{M}_1(s)\mathbb{N}_1(t)\mathbb{N}_2(t) \\ d_2 = \mathbb{W}(t) \\ d_3 = 0.58\mathbb{M}_2(s)\mathbb{N}_3(t)\mathbb{N}_4(t) \end{cases}$ where $\mathbb{M}_1(s) = \frac{K_{\xi_1}s}{s^2+2\epsilon_1\varepsilon_1 s+\varepsilon_1^2}$, $K_{\xi_1} = 0.26$, $\epsilon_1 = 0.5$, $\varepsilon_1 = 1.3$, and $\mathbb{N}_1(t) = 2.69$. Similarly, $\mathbb{M}_2(s) = \frac{K_{\xi_2}s}{s^2+2\epsilon_2\varepsilon_2 s+\varepsilon_2^2}$ with $K_{\xi_2} = 0.2$, $\epsilon_2 = 1.7$, $\varepsilon_2 = 0.9$, and $\mathbb{N}_3(t) = 1.56$, while the specific values of $\mathbb{N}_2(t), \mathbb{N}_4(t), \mathbb{W}(t)$ can be found in [37].

We simulate a 40% loss of effectiveness occurring after 30 s for the bow tunnel thruster and a stuck condition at $0.1\sin(2t)$ for aft tunnel thruster I.

For simulation, B_v is chosen as [37],$\gamma_0 = 1$ and $x(0) = [0.1\ \ -0.01\ \ -0.05\ 0.11\ -0.07\ 0.07]^T$, $\hat{\bar{w}}(0) = [0.5, -0.5, 0.01]$, $\hat{\mu}_0(0) = 0.1$, $\hat{\bar{u}}_s(0) = [0.12, 0.1, 0.1, 0.1, 0.1, 0.1]$, $\hat{\varrho}(0) = [0.05, 0.05, 0.05, 0.05, 0.05, 0.05]$, $\hat{\zeta}(0) = [0, 0, 0, 0, 0, 0]$, $\hat{\omega}(0) = [0.2, 0.1, -0.1, 0.2, 0]$, $\hat{\varphi}_0(0) = 0.1$, $\gamma = 10$, $\gamma_0 = [0.01, 0.01, 0.01, 0.01, 0.01, 0.01]$, $\gamma_1 = [0.001, 0.001, 0.001, 0.001, 0.001, 0.001] = \gamma_2$, $\gamma_3 = [0.023, 0.023, 0.023]$, $\gamma_4 = [1, 1, 1, 1, 1, 1]$, $\gamma_5 = 0.01$.

The simulation results presented in this paper affirm the effectiveness of the proposed control approach. Figure 3 illustrates the achieved state responses, demonstrating the convergence of the states to zero over time as proposed. Upon the occurrence of faults starting from $t = 30$ s, the states exhibit fluctuations due to the fault influence; however, they swiftly resume convergence to zero under the action of the fault-tolerant controller. Analysis of the control signals in Figure 4 further validates the efficacy of the proposed controller. It is observed that the controller promptly responds to fault occurrences at $t = 30$ s and adjusts accordingly. In sharp contrast, the controller design scheme proposed in [22] without fault tolerance consideration is evident. As depicted in Figures 5 and 6, it is clear that, after the occurrence of faults at $t = 30$ s, both the system states and the controller signals exhibit noticeable divergence. In summary, the control methodology outlined in Section 3 demonstrates commendable control performance. By selecting another set of parameters for random noise ocean disturbances, $K_{\xi_1} = 0.2$, $\epsilon_1 = 0.4$, $\varepsilon_1 = 0.7$, and $\mathbb{N}_1(t) = 3.2$. Similarly, $K_{\xi_2} = 0.6$, $\epsilon_2 = 1.6$, $\varepsilon_2 = 1$, and $\mathbb{N}_3(t) = 4.2$; we can obtain the result of Figure 7. In order to further demonstrate the robustness of the controller designed in this paper to disturbances, this paper further expands the types of disturbances and selects the following sine wave disturbances: $d_1 = \begin{cases} -0.8\sin(1.6t)e^{-0.15t} & t \in [0\text{ s}, 30\text{ s}) \\ -1.2\sin(1.6(t-30))e^{-0.15(t-30)} & \text{otherwise} \end{cases}$, $d_2 = \begin{cases} -0.6\cos(1.6t)e^{-0.12t} & t \in [0\text{ s}, 30\text{ s}) \\ -1.5\cos(1.6t)e^{-0.12(t-30)} & \text{otherwise} \end{cases}$, $d_3 = \begin{cases} \cos(t)e^{-0.08t} & t \in [0\text{ s}, 30\text{ s}) \\ \sin(t)e^{-0.08(t-30)} & \text{otherwise} \end{cases}$. From Figures 7 and 8, it is not difficult to see that the fault-tolerant control scheme proposed in this paper can still achieve good control effects under different disturbances. In order to further quantify the impact of disturbances on the behavior of the control system, this paper focuses on calculating the steady-state error of the output information starting from 10 s after the fault occurs, which is 40 s later. Table 2 shows the steady-state errors for each

disturbance scenario. Moreover, under ocean disturbance, our system's H_∞ performance index of 0.1 indicates better disturbance rejection compared with 0.2 in [48]. These comparisons demonstrate the effectiveness and robustness of our control approach. Compared with the traditional PID disturbance handling method, the control scheme provided in this article can easily handle disturbances and avoid the complicated process of adjusting PID parameters based on manual experience. To further explore the fault-tolerant capability of the fault-tolerant controller designed in this article, we once again simulated the situation where the bow and aft tunnel thrusters experienced 60% and 50% effectiveness losses simultaneously after 30 s, respectively. The results are shown in Figure 9.

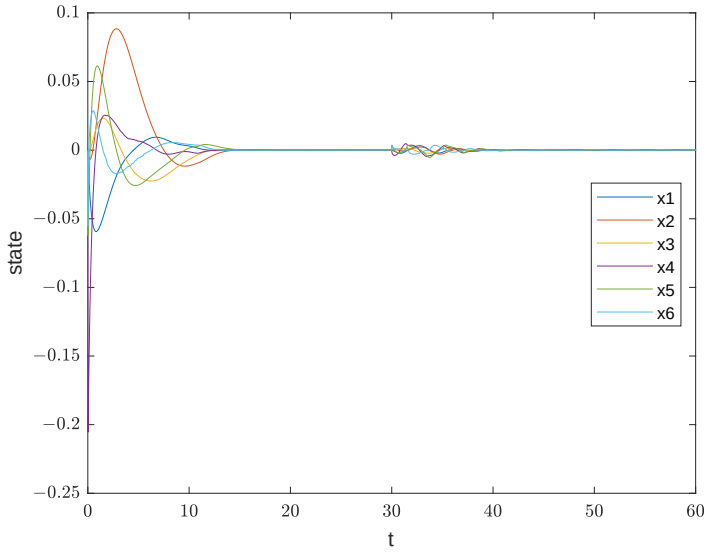

Figure 3. System responses $x(t)$ using the scheme developed in this paper.

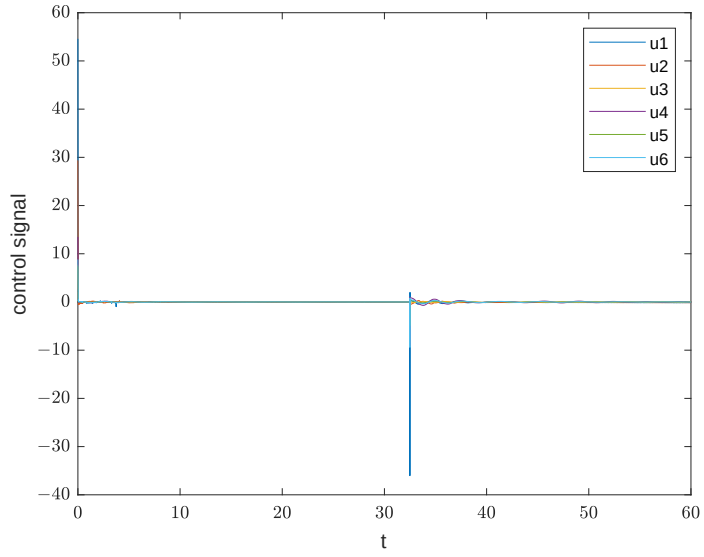

Figure 4. Controller responses $u(t)$ using the scheme developed in this paper.

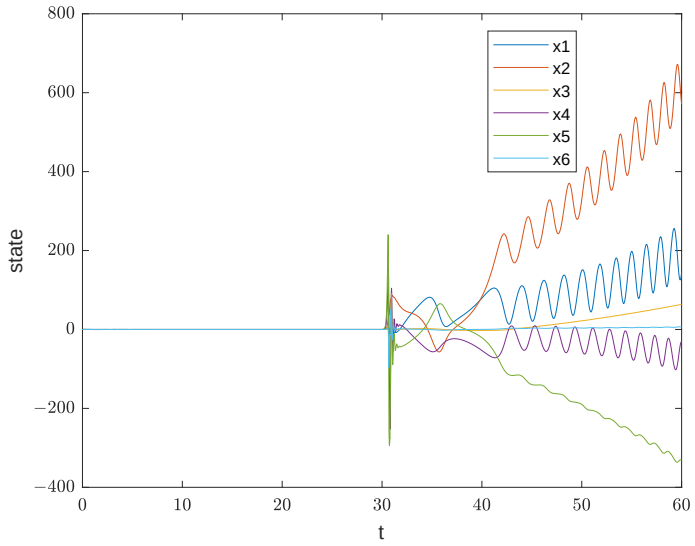

Figure 5. System responses $x(t)$ using the scheme developed in [22].

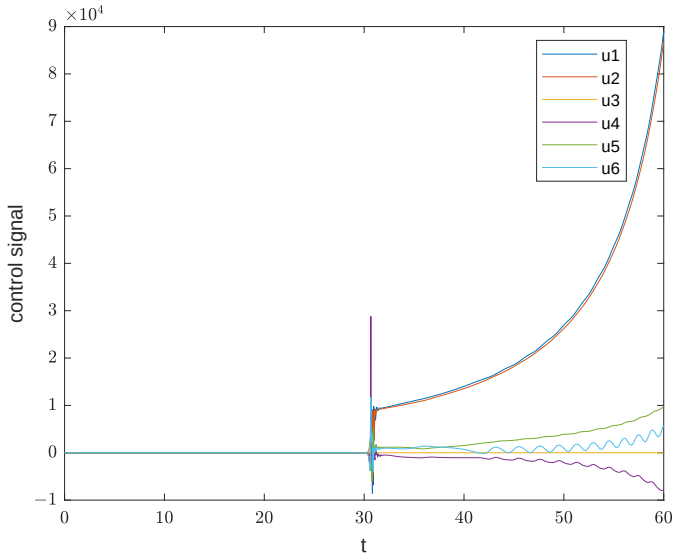

Figure 6. Controller responses $u(t)$ using the scheme developed [22].

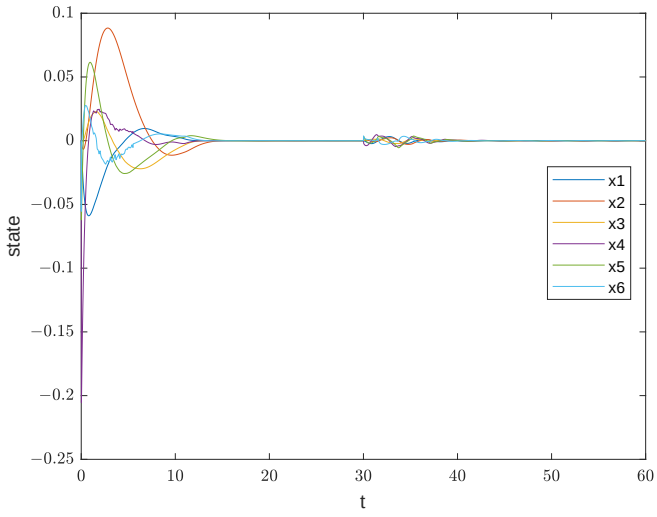

Figure 7. System responses $x(t)$ using the scheme developed in this paper with another set of parameters for random noise ocean disturbances.

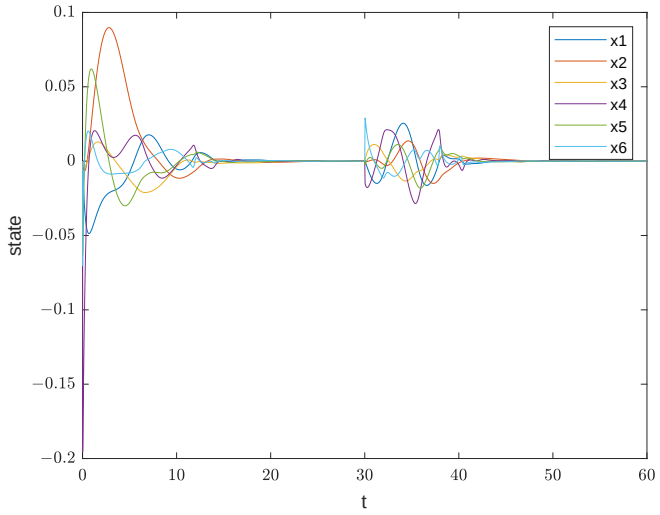

Figure 8. System responses $x(t)$ using the scheme developed in this paper with sine wave disturbances.

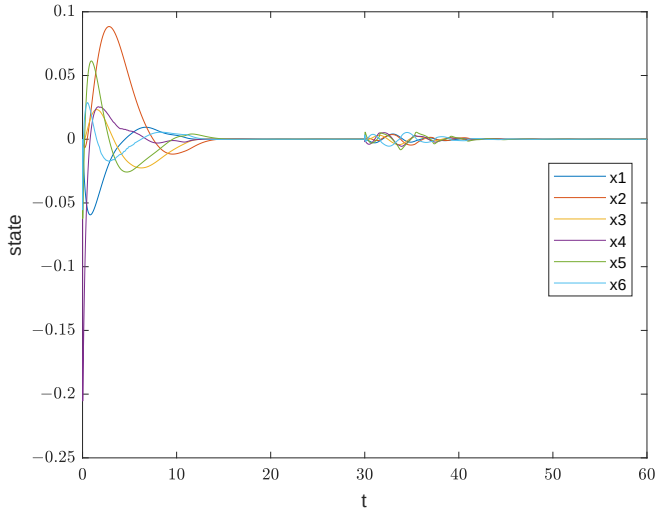

Figure 9. System responses $x(t)$ using the scheme developed in this paper with the bow and aft tunnel thrusters experiencing 60% and 50% effectiveness losses simultaneously.

Table 2. Table of steady-state error.

Type of Disturbance	$\mathbf{SteadyError_{y_1}}$	$\mathbf{SteadyError_{y_2}}$	$\mathbf{SteadyError_{y_3}}$
reference [22]	7.35×10^{-05}	6.13×10^{-05}	4.56×10^{-05}
random noise	7.49×10^{-05}	6.24×10^{-05}	4.65×10^{-05}
sine wave	8.83×10^{-05}	6.62×10^{-05}	6.95×10^{-05}

5. Conclusions

In this study, a fault-tolerant output feedback ISMC strategy is devised for T–S fuzzy UMVs subject to unknown premise variables. Initially, the T–S fuzzy UMV model incorporating unknown premise variables and actuator faults is established. Subsequently, to address the issue of unknown membership functions resulting from unknown premise variables, a compensator and a fault-tolerant controller based on a switching mechanism with upper and lower bounds of membership functions are designed. Adaptive RBFNN is utilized to approximate the nonlinear terms in the T–S fuzzy UMV model. The proposed method's effectiveness is confirmed by simulation results. Future research will focus on investigating delay and event-triggering issues in T–S fuzzy UMV DP systems.

Author Contributions: Conceptualization, L.H. and Y.W.; methodology, L.H. and Y.W.; software, If no software name appears in the text, please ignore; validation, Y.W. and L.H.; formal analysis, Y.W.; investigation, Y.W.; resources, L.H., T.L. and C.L.C.; data curation, Y.W.; writing—original draft preparation, Y.W.; writing—review and editing, Y.W. and X.Y.; visualization, Y.W.; supervision, L.H.; project administration, L.H.; funding acquisition, L.H., T.L. and C.L.C. All authors have read and agreed to the published version of the manuscript.

Funding: This work is supported in part by the National Natural Science Foundation of China (under Grant Nos. 51939001, 52171292, 61976033, 62003069); the LiaoNing Revitalization Talents Program (under Grant Nos. XLYC1908018, XLYC1807046); the Dalian Outstanding Young Talents Program (under Grant No. 2022RJ05), and the Science and Technology Development Fund, Macau SAR (File no. SKL-IOTSC-2018-2020, 0018/2019/AKP).

Institutional Review Board Statement: Not applicable.

Informed Consent Statement: Not applicable.

Data Availability Statement: Data are contained within the article.

Conflicts of Interest: The authors declare no conflicts of interest.

References

1. Shirakura, N.; Kiyokawa, T.; Kumamoto, H.; Takamatsu, J.; Ogasawara, T. Collection of Marine Debris by Jointly Using UAV-UUV with GUI for Simple Operation. *IEEE Access* **2021**, *9*, 67432–67443. [CrossRef]
2. Shah, B.C.; Gupta, S.K. Long-Distance Path Planning for Unmanned Surface Vehicles in Complex Marine Environment. *IEEE J. Ocean. Eng.* **2020**, *45*, 813–830. [CrossRef]
3. Wiig, M.S.; Pettersen, K.Y.; Krogstad, T.R. Collision Avoidance for Underactuated Marine Vehicles Using the Constant Avoidance Angle Algorithm. *IEEE Trans. Control Syst. Technol.* **2020**, *28*, 951–966. [CrossRef]
4. Han, J.; Cho, Y.; Kim, J. Coastal SLAM with Marine Radar for USV Operation in GPS-Restricted Situations. *IEEE J. Ocean. Eng.* **2019**, *44*, 300–309. [CrossRef]
5. Mendoza-Chok, J.; Luque, J.C.C.; Salas-Cueva, N.F.; Yanyachi, D.; Yanyachi, P.R. Hybrid Control Architecture of an Unmanned Surface Vehicle Used for Water Quality Monitoring. *IEEE Access* **2022**, *10*, 112789–112798. [CrossRef]
6. Moghimi, M.K.; Mohanna, F. Reliable Object Recognition Using Deep Transfer Learning for Marine Transportation Systems with Underwater Surveillance. *IEEE Trans. Intell. Transp. Syst.* **2023**, *24*, 2515–2524. [CrossRef]
7. Pugi, L.; Pagliai, M.; Allotta, B. A robust propulsion layout for underwater vehicles with enhanced manoeuvrability and reliability features. *Proc. Inst. Mech. Eng. Part M J. Eng. Marit. Environ.* **2018**, *232*, 358–376. [CrossRef]
8. Yu, Y.; Guo, C.; Li, T. Finite-Time LOS Path Following of Unmanned Surface Vessels with Time-Varying Sideslip Angles and Input Saturation. *IEEE/ASME Trans. Mechatron.* **2022**, *27*, 463–474. [CrossRef]
9. Yao, Q. Fixed-time trajectory tracking control for unmanned surface vessels in the presence of model uncertainties and external disturbances. *Int. J. Control* **2022**, *95*, 1133–1143. [CrossRef]
10. Liao, Y.; Jiang, Q.; Du, T.; Jiang, W. Redefined output model-free adaptive control method and unmanned surface vehicle heading control. *IEEE J. Ocean. Eng.* **2019**, *45*, 714–723. [CrossRef]
11. Fossen, T.I. Guidance and Control of Ocean Vehicles. Ph.D. Thesis, University of Trondheim, Trondheim, Norway, 1999; ISBN 0-471-94113 1.
12. Roberts, G.N.; Sutton, R. *Advances in Unmanned Marine Vehicles*, 1st ed.; Institution of Engineering and Technology: London, UK, 2006.
13. Kahveci, N.E.; Ioannou, P.A. Adaptive steering control for uncertain ship dynamics and stability analysis. *Automatica* **2013**, *49*, 685–697. [CrossRef]
14. Wang, Y.L.; Han, Q.L. Network-based modelling and dynamic output feedback control for unmanned marine vehicles in network environments. *Automatica* **2018**, *91*, 43–53. [CrossRef]
15. Rogne, R.H.; Bryne, T.H.; Fossen, T.I.; Johansen, T.A. On the Usage of Low-Cost MEMS Sensors, Strapdown Inertial Navigation, and Nonlinear Estimation Techniques in Dynamic Positioning. *IEEE J. Ocean. Eng.* **2021**, *46*, 24–39. [CrossRef]
16. Ning, J.; Li, T.; Chen, C.P. Neuro-adaptive distributed formation tracking control of under-actuated unmanned surface vehicles with input quantization. *Ocean Eng.* **2022**, *265*, 112492. [CrossRef]
17. Ma, L.; Wang, Y.L.; Han, Q.L. Event-Triggered Dynamic Positioning for Mass-Switched Unmanned Marine Vehicles in Network Environments. *IEEE Trans. Cybern.* **2022**, *52*, 3159–3171. [CrossRef] [PubMed]
18. Liang, H.; Li, H.; Gao, J.; Cui, R.; Xu, D. Economic MPC-Based Planning for Marine Vehicles: Tuning Safety and Energy Efficiency. *IEEE Trans. Ind. Electron.* **2023**, *70*, 10546–10556. [CrossRef]
19. Wang, R.; Li, H.; Liang, B.; Shi, Y.; Xu, D. Policy Learning for Nonlinear Model Predictive Control with Application to USVs. *IEEE Trans. Ind. Electron.* **2024**, *71*, 4089–4097. [CrossRef]
20. Chang, W.; Liang, H.; Ku, C. Fuzzy controller design subject to actuator saturation for dynamic ship positioning systems with multiplicative noises. *Proc. Inst. Mech. Eng. Part I J. Syst. Control Eng.* **2010**, *224*, 725–736. [CrossRef]

21. Ngongi, W.E.; Du, J.; Wang, R. Robust fuzzy controller design for dynamic positioning system of ships. *Int. J. Control Autom. Syst.* **2015**, *13*, 1294–1305. [CrossRef]
22. Wang, Y.L.; Han, Q.L.; Fei, M.R.; Peng, C. Network-Based T-S Fuzzy Dynamic Positioning Controller Design for Unmanned Marine Vehicles. *IEEE Trans. Cybern.* **2018**, *48*, 2750–2763. [CrossRef]
23. Wang, Y.; Li, T.; Wu, Y.; Yang, X.; Chen, C.; Long, Y.; Yang, Z.; Ning, J. L_∞ Fault Estimation and Fault-Tolerant Control for Nonlinear Systems by T-S Fuzzy Model Method with Local Nonlinear Models. *Int. J. Fuzzy Syst.* **2021**, *23*, 1714–1727. [CrossRef]
24. Lin, X.; Nie, J.; Jiao, Y.; Liang, K.; Li, H. Nonlinear adaptive fuzzy output-feedback controller design for dynamic positioning system of ships. *Ocean Eng.* **2018**, *158*, 186–195. [CrossRef]
25. Hao, L.Y.; Zhang, H.; Guo, G.; Li, H. Quantized Sliding Mode Control of Unmanned Marine Vehicles: Various Thruster Faults Tolerated with a Unified Model. *IEEE Trans. Syst. Man Cybern. Syst.* **2021**, *51*, 2012–2026. [CrossRef]
26. Hao, L.Y.; Yu, Y.; Li, H. Fault tolerant control of UMV based on sliding mode output feedback. *Appl. Math. Comput.* **2019**, *359*, 433–455. [CrossRef]
27. Wang, Y.; Jiang, B.; Wu, Z.G.; Xie, S.; Peng, Y. Adaptive Sliding Mode Fault-Tolerant Fuzzy Tracking Control with Application to Unmanned Marine Vehicles. *IEEE Trans. Syst. Man Cybern. Syst.* **2021**, *51*, 6691–6700. [CrossRef]
28. Hao, W.; Xian, B.; Xie, T. Fault-Tolerant Position Tracking Control Design for a Tilt Tri-Rotor Unmanned Aerial Vehicle. *IEEE Trans. Ind. Electron.* **2022**, *69*, 604–612. [CrossRef]
29. Van, M.; Ge, S.S. Adaptive Fuzzy Integral Sliding-Mode Control for Robust Fault-Tolerant Control of Robot Manipulators with Disturbance Observer. *IEEE Trans. Fuzzy Syst.* **2021**, *29*, 1284–1296. [CrossRef]
30. Wang, Z.; Li, Q.; Li, S. Adaptive integral-type terminal sliding mode fault tolerant control for spacecraft attitude tracking. *IEEE Access* **2019**, *7*, 35195–35207. [CrossRef]
31. Mazare, M.; Taghizadeh, M.; Ghaf-Ghanbari, P. Fault-tolerant control based on adaptive super-twisting nonsingular integral-type terminal sliding mode for a delta parallel robot. *J. Braz. Soc. Mech. Sci. Eng.* **2020**, *42*, 443. [CrossRef]
32. Yu, X.N.; Hao, L.Y. Integral sliding mode fault tolerant control for unmanned surface vessels with quantization: Less iterations. *Ocean Eng.* **2022**, *260*, 111820. [CrossRef]
33. Hao, L.Y.; Zhang, Y.Q.; Shen, C.; Xu, F. Fault-Tolerant Control for Unmanned Marine Vehicles via Quantized Integral Sliding Mode Output Feedback Technique. *IEEE Trans. Intell. Transp. Syst.* **2023**, *24*, 5014–5023. [CrossRef]
34. Ijaz, S.; Galea, M.; Hamayun, M.T.; Ijaz, H.; Javaid, U. A new output integral sliding mode fault-tolerant control and fault estimation scheme for uncertain systems. *IEEE Trans. Autom. Sci. Eng.* **2023**, 1–12. [CrossRef]
35. Chang, J.L. Dynamic output integral sliding-mode control with disturbance attenuation. *IEEE Trans. Autom. Control* **2009**, *54*, 2653–2658. [CrossRef]
36. Hao, L.Y.; Zhang, Y.Q.; Li, H. Fault-tolerant control via integral sliding mode output feedback for unmanned marine vehicles. *Appl. Math. Comput.* **2021**, *401*, 126078. [CrossRef]
37. Wang, Y.; Hao, L.Y.; Li, T.; Chen, C.P. Integral sliding mode-based fault-tolerant control for dynamic positioning of unmanned marine vehicles based on a T-S fuzzy model. *J. Mar. Sci. Eng.* **2023**, *11*, 370. [CrossRef]
38. Song, W.; Li, Y.; Tong, S. Fuzzy Finite-Time H_∞ Hybrid-Triggered Dynamic Positioning Control of Nonlinear Unmanned Marine Vehicles Under Cyber-Attacks. *IEEE Trans. Intell. Veh.* **2023**, *9*, 970–980. [CrossRef]
39. Huang, S.J.; Yang, G.H. Fault tolerant controller design for T–S fuzzy systems with time-varying delay and actuator faults: A K-step fault-estimation approach. *IEEE Trans. Fuzzy Syst.* **2014**, *22*, 1526–1540. [CrossRef]
40. Han, H.; Yang, Y.; Li, L.; Ding, S.X. Performance-based fault detection and fault-tolerant control for nonlinear systems with T–S fuzzy implementation. *IEEE Trans. Cybern.* **2019**, *51*, 801–814. [CrossRef]
41. Li, H.; Xu, J.; Yu, J. Discrete event-triggered fault-tolerant control of underwater vehicles based on Takagi–Sugeno fuzzy model. *IEEE Trans. Syst. Man Cybern. Syst.* **2022**, *53*, 1841–1851. [CrossRef]
42. Li, X.J.; Yang, G.H. Fault detection for T-S fuzzy systems with unknown membership functions. *IEEE Trans. Fuzzy Syst.* **2013**, *22*, 139–152. [CrossRef]
43. Li, X.J.; Yang, G.H. Finite Frequency L_2-L_∞ Filtering of TS Fuzzy Systems with Unknown Membership Functions. *IEEE Trans. Syst. Man Cybern. Syst.* **2016**, *47*, 1884–1897. [CrossRef]
44. Arioui, H.; Nehaoua, L. Unknown Dynamics Decoupling to Overcome Unmeasurable Premise Variables in Takagi–Sugeno Observer Design. *IEEE Control Syst. Lett.* **2020**, *5*, 61–66. [CrossRef]
45. Yan, J.J.; Yang, G.H.; Li, X.J. Fault detection in finite frequency domain for TS fuzzy systems with partly unmeasurable premise variables. *Fuzzy Sets Syst.* **2021**, *421*, 158–177. [CrossRef]
46. Dong, J.; Yang, G.H. Observer-based output feedback control for discrete-time TS fuzzy systems with partly immeasurable premise variables. *IEEE Trans. Syst. Man Cybern. Syst.* **2016**, *47*, 98–110. [CrossRef]
47. Li, H.; Wu, C.; Jing, X.; Wu, L. Fuzzy tracking control for nonlinear networked systems. *IEEE Trans. Cybern.* **2016**, *47*, 2020–2031. [CrossRef]
48. Hao, L.Y.; Zhang, H.; Li, T.S.; Lin, B.; Chen, C.L.P. Fault Tolerant Control for Dynamic Positioning of Unmanned Marine Vehicles Based on T-S Fuzzy Model with Unknown Membership Functions. *IEEE Trans. Veh. Technol.* **2021**, *70*, 146–157. [CrossRef]
49. Fossen, T.I.; Sagatun, S.I.; Sørensen, A.J. Identification of dynamically positioned ships. *Control Eng. Pract.* **1996**, *4*, 369–376. [CrossRef]

50. Zou, Y.; Zheng, Z. A Robust Adaptive RBFNN Augmenting Backstepping Control Approach for a Model-Scaled Helicopter. *IEEE Trans. Control Syst. Technol.* **2015**, *23*, 2344–2352. [CrossRef]
51. Jabbari, F.; Benson, R. Observers for stabilization of systems with matched uncertainty. *Dyn. Control* **1992**, *2*, 303–323. [CrossRef]
52. Edwards, C.; Spurgeon, S. *Sliding Mode Control: Theory and Applications*, 1st ed.; CRC Press: London, UK, 1998.